Cortical mapping by Laplace-Cauchy transmission using a boundary element method.

Maureen Clerc, Jan Kybic

Cortical mapping by Laplace-Cauchy transmission using a boundary element method.

Maureen Clerc[1] **and Jan Kybic**[2]

[1] Odyssée Project-Team
INRIA, ENPC, ENS Ulm, France
[2]Center for Machine Perception,
Czech Technical University, Prague, Czech Republic

Abstract. The Laplace-Cauchy problem of propagating Dirichlet and Neumann data from a portion to the rest of the boundary is an ill-posed inverse problem. Many regularizing algorithms have been recently proposed, in order to stabilize the solution with respect to noisy or incomplete data. Our main application is in electroencephalography (EEG) where potential measurements available at part of the scalp are used to reconstruct the potential and the current on the inner skull surface. This problem, known as cortical mapping, and other applications — in fields such as nondestructive testing, or biomedical engineering — require to solve the problem in realistic, three-dimensional geometry. The goal of this article is to present a new boundary element based method for solving the Laplace-Cauchy problem in three dimensions, in a multilayer geometry. We validate the method experimentally on simulated data.

1. Introduction

The transmission of Cauchy data for the Laplace problem consists in estimating a function V, harmonic within a domain D, from the values of V and its normal derivative $\partial_{\mathbf{n}} V$ on the boundary ∂D. This ill-posed problem has numerous applications in engineering, whether mechanical, electrical or biomedical. Examples include functional brain imaging [4], crack or inclusion identification [5], heat conduction [8], corrosion identification [17].

The Holmgren theorem guarantees uniqueness of the Cauchy continuation problem, if the data is perfectly known on a dense subset of the boundary. This is however never the case in practice, and causes instability. Many methods have been proposed to regularize the Cauchy problem, among which an energy-minimizing approach [2], methods using quasi-reversibility [18],[11], and methods alternating Dirichlet and Neumann problems, with regularizing properties [19],[7],[3]. The present work is based on a boundary element discretization, and uses a Tikhonov-type regularization.

Electroencephalographic data (EEG) measured on the scalp suffer from a smoothing effect of the skull, which acts as a spatial low-pass filter. Surface Laplacian methods are often used to sharpen the data, but they do not take into account the 3D head geometry of the particular subject [23]. Cortical mapping methods are therefore needed, that aim to reconstruct electric field inside the brain from the surface measurements, taking advantage of the physical model for a specific subject.

Our approach is similar to a boundary element method proposed for the Cauchy problem in EEG [16]. However, the present method is based on a mixed formulation, involving both the potential and its normal derivative. The mixed formulation significantly improves the precision and robustness of the forward EEG problem (calculating the electric potential from known sources inside the brain) [20] and should therefore also improve the accuracy and robustness of the inverse problem, cortical mapping. Another distinguishing feature of our method is the use of the harmonic lift [12] to convert the constrained problem into an easy to solve, unconstrained one.

We present the mixed boundary element approach in Section 2, and show that the solution must belong to the kernel $\mathcal{N}(\mathcal{H})$ of a linear operator H. In Section 3, the solution is sought as the minimizer within $\mathcal{N}(\mathcal{H})$ of a Tikhonov-like term, involving a norm of the difference between the measured data and the simulations, as well as regularizing terms. In Section 4, we apply the method to a cortical mapping problem, on simulated three-dimensional EEG data.

2. A mixed boundary element formulation

2.1. Geometrical setting, and notation

Our Cauchy transmission is defined in the context of electrostatics, where the electric potential in a conducting volume D is related to an electrical source g by a Poisson equation

$$\nabla \cdot (\sigma \nabla V) = g.$$

The 3D geometrical setting is depicted as a cross-section in Figure 1. The domain D is composed of a collection of open subdomains Ω_i such that $\overline{D} = \cup_{i=1}^{N+1} \overline{\Omega}_i$. Each subdomain Ω_i represents a volume of homogeneous conductivity σ_i. The volumes Ω_i are nested inside one another, and we denote the interfaces between neighboring conductors by $S_i = \overline{\Omega}_i \cap \overline{\Omega}_{i+1}$. By extension, ∂D is denoted S_0 (see Figure 1).

This model can be extended to more general geometrical settings, in which volumes of constant conductivity are not nested [21] at the expense of notational simplicity.

Our geometrical setting is suited to EEG, where measurements are made on scalp electrodes, and electrical activity is confined within the brain. In Section 4, numerical experiments are conducted on a three-layer model.

The support of the source term g is restricted to the innermost domain Ω_{N+1}. In other Ω_i, the potential V satisfies a homogeneous Laplace equation,

$$\Delta V = 0 \text{ in } \Omega_i, \qquad \text{for } i = 1, \ldots, N \tag{1}$$

with jump conditions,

$$[V]_i \quad = 0 \ , \tag{2}$$

$$[\sigma \partial_{\mathbf{n}} V]_i = 0 \qquad \text{for } i = 1, \ldots, N-1. \tag{3}$$

The jump of a function f across surface S_i is denoted $[f]_{S_i} = f^-_{S_i} - f^+_{S_i}$, with the inner and outer limits f^-, f^+ defined as:

$$f^{\pm}_{S_i}(\mathbf{r}) = \lim_{\alpha \to 0^{\pm}} f(\mathbf{r} + \alpha \mathbf{n}), \text{ for } \mathbf{r} \text{ on } S_i,$$

relative to the orientation of a normal vector $\mathbf{n}$ (see Figure 1). If f is continuous across S_i, its restriction to S_i is denoted f_{S_i}.

The exterior of D is considered to be non-conductive ($\sigma_0 = 0$), hence the boundary condition $\partial_{\mathbf{n}} V = 0$ is imposed on ∂D. The goal of the multilayer Cauchy transmission problem is to compute $V_{S_i} = V$ and $p_{S_i} = p = \sigma \partial_{\mathbf{n}} V$ on all interfaces S_i, $i = 0, \ldots, n$ from a set of discrete measurements of V on the boundary S_0.

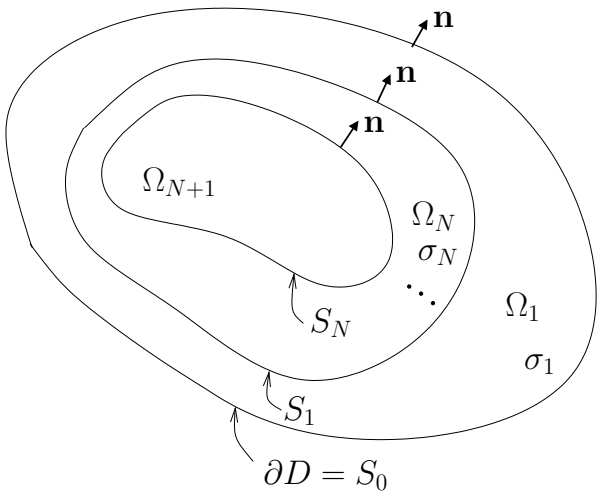

Figure 1. The domain D is modeled as a set of nested regions $\Omega_1, \ldots, \Omega_{N+1}$ with constant conductivities $\sigma_1, \ldots, \sigma_{N+1}$, separated by interfaces $S_1, \ldots, S_N$. Arrows indicate the outward normal directions $\mathbf{n}$.

2.2. Integral representation theorem

Given a bounded domain Ω in $\mathbb{R}^3$ with regular boundary $\partial\Omega$, we can define four classical boundary integral operators [22]: the double-layer operator $\mathcal{D}$

$$(\mathcal{D}f)(\mathbf{r}) = \int_{\partial\Omega} \partial_{\mathbf{n}'} G(\mathbf{r}-\mathbf{r}') f(\mathbf{r}')\, \mathrm{d}s(\mathbf{r}')$$

where $\mathbf{n}'$ represents the surface normal at $\mathbf{r}'$ and $G(\mathbf{r}) = \frac{1}{4\pi\|\mathbf{r}\|}$ is the Green function for the Laplace equation, such that $-\Delta G = \delta_0$; the transpose $\mathcal{D}^*$ of $\mathcal{D}$ in $L^2(\partial\Omega)$

$$(\mathcal{D}^* f)(\mathbf{r}) = \int_{\partial\Omega} \partial_{\mathbf{n}} G(\mathbf{r}-\mathbf{r}') f(\mathbf{r}')\, \mathrm{d}s(\mathbf{r}') \ ,$$

the single-layer operator $\mathcal{S}$

$$(\mathcal{S}f)(\mathbf{r}) = \int_{\partial\Omega} G(\mathbf{r}-\mathbf{r}') f(\mathbf{r}')\, \mathrm{d}s(\mathbf{r}') \ ,$$

and the higher-order operator $\mathcal{N}$

$$(\mathcal{N}f)(\mathbf{r}) = \int_{\partial\Omega} \partial^2_{\mathbf{n},\mathbf{n}'} G(\mathbf{r}-\mathbf{r}') f(\mathbf{r}')\, \mathrm{d}s(\mathbf{r}') \ .$$

To avoid inherent ambiguity of the potential u at infinity, a decay condition $\mathcal{H}$ is introduced:

$$\begin{cases} \lim\limits_{r\to\infty} r\,|u(\mathbf{r})| < \infty \\ \lim\limits_{r\to\infty} r \dfrac{\partial u}{\partial r}(\mathbf{r}) = 0 \end{cases}$$

where $r = \|\mathbf{r}\|$, and $\frac{\partial u}{\partial r}(\mathbf{r})$ denotes the partial derivative of u in the radial direction.

The classical fundamental representation theorem [22] shows that a harmonic function u in a domain is completely determined by its value and derivative on a boundary. More specifically:

Theorem 1 (Representation Theorem) *Let u be a harmonic function in $\mathbb{R}^3\backslash\partial\Omega$ satisfying the decay condition $\mathcal{H}$. Then on $\partial\Omega$,*

$$\begin{aligned} -\partial_{\mathbf{n}} u^{\pm} &= \pm \frac{[\partial_{\mathbf{n}} u]_{\partial\Omega}}{2} + \mathcal{N}[u]_{\partial\Omega} - \mathcal{D}^*[\partial_{\mathbf{n}} u]_{\partial\Omega} \\ u^{\pm} &= \mp \frac{[u]_{\partial\Omega}}{2} - \mathcal{D}[u]_{\partial\Omega} + \mathcal{S}[\partial_{\mathbf{n}} u]_{\partial\Omega} \end{aligned} \tag{4}$$

2.3. Succession of Harmonic Problems

To find a solution V of (1),(2),(3), we apply the representation theorem in each subdomain Ω_i to obtain a set of coupled boundary integral equations involving V_{S_i} and $p_{S_i} = (\sigma\partial_{\mathbf{n}} V)_{S_i}$. The method has been presented in [20] for the forward problem of electroencephalography.

The following proposition provides $2N$ constraints satisfied by the variables V_{S_0}, p_{S_0}, ..., V_{S_N}, p_{S_N}. We introduce a notation $\mathcal{D}_{i,j}$, $\mathcal{S}_{i,j}$, $\mathcal{N}_{i,j}$ for the restrictions of operators $\mathcal{D}$, $\mathcal{S}$, $\mathcal{N}$; for example $\mathcal{D}_{i,j}$ acts on a function defined on S_j, and produces a function defined on S_i.

Proposition 1 *Considering the geometrical setting of Figure 1, let V satisfy $\nabla\cdot(\sigma\,\nabla V) = 0$ in $\mathbb{R}^3\backslash\overline{\Omega}_{N+1}$. Then the restrictions of V and $\sigma\partial_{\mathbf{n}} V$ to S_i, $i = 0,\ldots,N$, denoted V_{S_i} and p_{S_i}, satisfy the following set of coupled boundary integral equations: for $i = 1,\ldots,N$,*

$$\begin{aligned} &\mathcal{D}_{i,i-1} V_{S_{i-1}} - 2\,\mathcal{D}_{i,i} V_{S_i} + \mathcal{D}_{i,i+1} V_{S_{i+1}} - \\ &\qquad \frac{1}{\sigma_i}\mathcal{S}_{i,i-1} p_{S_{i-1}} + \left(\frac{1}{\sigma_i} + \frac{1}{\sigma_{i+1}}\right) S_{i,i} p_{S_i} - \frac{1}{\sigma_{i+1}}\mathcal{S}_{i,i+1} p_{S_{i+1}} = 0\ , \end{aligned} \tag{5}$$

$$\begin{aligned} &\sigma_i \mathcal{N}_{i,i-1} V_{S_{i-1}} - (\sigma_i + \sigma_{i+1})\mathcal{N}_{i,i} V_{S_i} + \sigma_{i+1}\mathcal{N}_{i,i+1} V_{S_{i+1}} - \\ &\qquad \mathcal{D}^*_{i,i-1} p_{S_{i-1}} + 2\,\mathcal{D}^*_{i,i} p_{S_i} - \mathcal{D}^*_{i,i+1} p_{S_{i+1}} = 0\ . \end{aligned} \tag{6}$$

Proof Consider a set of harmonic functions $\{u_i; i = 1,\ldots,N\}$ in $\mathbb{R}^3\backslash\partial\Omega_i$, such that

$$u_i = \begin{cases} V & \text{in } \Omega_i \\ 0 & \text{in } \mathbb{R}^3\backslash\overline{\Omega}_i \end{cases}\ .$$

Applying the integral representation theorem (4) to u_i inside Ω_i

$$(u_i)^+_{S_i} = -\frac{[u_i]_{\partial\Omega_i}}{2} - \mathcal{D}_{\partial\Omega_i}[u_i]_{\partial\Omega_i} + \mathcal{S}_{\partial\Omega_i}[\partial_{\mathbf{n}} u_i]_{\partial\Omega_i}\ . \tag{7}$$

Since the boundary $\partial\Omega_i$ is composed of two non-connected surfaces $S_i \cup S_{i-1}$, operators and functions defined on $\partial\Omega_i$ can be decomposed as:

$$\mathcal{D}_{\partial\Omega_i} f_{\partial\Omega_i} = \mathcal{D}_{i,i} f_{S_i} + \mathcal{D}_{i,i-1} f_{S_{i-1}} + \mathcal{D}_{i-1,i} f_{S_i} + \mathcal{D}_{i-1,i-1} f_{S_{i-1}}\ .$$

The flow, $p = \sigma \partial_{\mathbf{n}} V$ is a continuous quantity across each interface S_i, satisfying‡

$$[u_i]_{S_i} = -V_{S_i} \qquad [\partial_{\mathbf{n}} u_i]_{S_i} = -(\partial_{\mathbf{n}} V)_{S_i} = -p_{S_i}/\sigma_i,$$
$$[u_i]_{S_{i-1}} = V_{S_{i-1}} \qquad [\partial_{\mathbf{n}} u_i]_{S_{i-1}} = (\partial_{\mathbf{n}} V)_{S_{i-1}} = p_{S_{i-1}}/\sigma_i \ .$$

Inserting these relations into (7) yields

$$\frac{V_{S_i}}{2} + \mathcal{D}_{i,i-1} V_{S_{i-1}} - \mathcal{D}_{i,i} V_{S_i} - \mathcal{S}_{i,i-1} \frac{p_{S_{i-1}}}{\sigma_i} + \mathcal{S}_{i,i} \frac{p_{S_i}}{\sigma_i} = 0 \ . \tag{8}$$

The integral representation theorem (4) is then applied to u_{i+1} on surface S_i

$$(u_{i+1})^-_{S_i} = \frac{[u_{i+1}]_{S_i}}{2} - \mathcal{D}_{\partial\Omega_{i+1}} [u_{i+1}]_{\partial\Omega_{i+1}} + \mathcal{S}_{\partial\Omega_{i+1}} [\partial_{\mathbf{n}} u_{i+1}]_{\partial\Omega_{i+1}}$$

which, after similar manipulations, becomes

$$\frac{V_{S_i}}{2} + \mathcal{D}_{i,i} V_{S_i} - \mathcal{D}_{i,i+1} V_{S_{i+1}} - \mathcal{S}_{i,i} \frac{p_{S_i}}{\sigma_{i+1}} + \mathcal{S}_{i,i+1} \frac{p_{S_{i+1}}}{\sigma_{i+1}} = 0 \ . \tag{9}$$

The desired result (5) is obtained by subtracting (8) and (9). The same treatment, applied to the second equation of the integral representation theorem, yields (6).

□

2.4. Discretization

The boundary integral formulation is "mixed" because it involves two types of variables: a potential V, and its flux $p = \sigma \partial_{\mathbf{n}} V$. The system of boundary integral equations is discretized using a Galerkin method, with P_1 (piecewise linear) surface elements for the potential and P_0 (piecewise constant) surface elements for the flux [10]. Details on discretization can be found in the article presenting the symmetric Boundary Element method for EEG [20].

We group all the discretized variables into a single vector X, which hence represents the collection of potentials and fluxes over all interfaces, in their P_1/P_0 discretization:

$$X = (V_N; p_N; V_{N-1}; p_{N-1}; \dots V_0)^T$$

Discretizing equations (5) and (6) for $i = 0$ to $N-1$, we obtain a linear system:

$$H\, X = 0 \ . \tag{10}$$

For a three-layer model ($N = 2$), we have

$$X = (V_2; p_2; V_1; p_1; V_0)^T$$

and $H\, X = 0$ takes the form

$$\begin{pmatrix} \sigma_2 \mathsf{N}_{12} & -\mathsf{D}^*_{12} & (\sigma_1+\sigma_2)\mathsf{N}_{11} & 2\mathsf{D}^*_{11} & \sigma_1 \mathsf{N}_{10} \\ -\mathsf{D}_{12} & \frac{1}{\sigma_2}\mathsf{S}_{12} & 2\mathsf{D}_{11} & -\left(\frac{1}{\sigma_1}+\frac{1}{\sigma_2}\right)\mathsf{S}_{11} & -\mathsf{D}_{10} \\ 0 & 0 & \sigma_1 \mathsf{N}_{01} & -\mathsf{D}^*_{01} & -\sigma_1 \mathsf{N}_{11} \end{pmatrix} \begin{pmatrix} V_2 \\ p_2 \\ V_1 \\ p_1 \\ V_0 \end{pmatrix} = \begin{pmatrix} 0 \\ 0 \\ 0 \end{pmatrix} \ .$$

We will consider this three-layer model in the numerical examples in Section 4.

‡ with the orientation convention of Figure 1

3. Regularization of the transmission problem

The discrete Cauchy transmission problem amounts to recovering the vector

$$X = (V_N; p_N; V_{N-1}; p_{N-1}; \ldots; V_0)^T \tag{11}$$

from the values of the potential at sensor positions on the outer surface. This notoriously ill-posed problem is subject to many sources of numerical instability: (1) the number of measurements is much smaller than the number of unknowns describing the electric field, (2) the measurements are not acquired over the whole boundary, but on a set of sensors, whose positions are not accurately known, (3) the measurements are subject to noise, and (4) the conductivity model is only an approximation of the physical reality. We present in this section a Tikhonov-type method, in which a cost function is minimized, composed of a measurement term and a regularization term. The originality of our approach is to impose the harmonic constraint in a hard manner.

The potential must satisfy $\Delta V = 0$ in each domain Ω_i, $i = 1, \ldots, n$, with continuity conditions for V (2) and for $p = \sigma \partial_{\mathbf{n}} V$ (3). Section 2 has shown that this harmonic constraint is represented by the linear system $H\,X = 0$. This is called "harmonic lift" in [12].

A way to impose that $H\,X = 0$ is to require that X be of the form $X = P_{\mathcal{N}(H)}\,Y$, where $P_{\mathcal{N}(H)}$ is the orthogonal projector onto the null-space of H. The projector $P_{\mathcal{N}(H)}$ is computed from H by singular value decomposition [14], as detailed in Algorithm 1.

Algorithm 1 NullSpaceProjector(S_0, S_1, $\ldots S_N$, σ_1, $\ldots$,σ_N)

Inputs: meshes of surfaces S_0, S_1, $\ldots S_N$, conductivities σ_1, $\ldots$, σ_N

Assemble H, matrix of dimensions $N_L \times N_C$

Perform Singular Value Decomposition of H:

$$H = U\,S\,W'$$

Return $P_{\mathcal{N}(H)}$ submatrix of W composed of its $N_C - N_L$ last columns

We introduce an interpolation matrix M transforming the potential values on the mesh nodes to the linearly interpolated values at sensor coordinates. The actual boundary measurements are denoted by m. To account for measurement noise and uncertainty on sensor positions, instead of requiring that $MX = m$ hold exactly, we minimize the residual term

$$M(X) = \|MX - m\|^2.$$

The ill-posedness of the Cauchy problem is addressed by incorporating a regularization term to the cost function to be minimized. Since our solution is discretized on a set of surfaces, we chose to control a norm of its surface gradient, which is the projection of the gradient on the tangent plane to the surface. Regularization using a gradient norm is a common practice in image restoration. As detailed in [1], for

a potential V discretized with P_1 elements, the L^2 norm of the surface gradient of V can be approximated as the sum of three terms, corresponding to orthogonal directions in $\mathbb{R}^3$:

$$S_V(X) = \|G^1 X\|^2 + \|G^2 X\|^2 + \|G^3 X\|^2.$$

Likewise, a norm of the surface variations of the flux is introduced, imposing a smoothness constraint on p, under the form

$$S_p(X) = \|J^1 X\|^2 + \|J^2 X\|^2 + \|J^3 X\|^2.$$

The regularity constraint is thus composed of the sum $\sum_{i=1}^{3} \alpha_V \|G^i X\|^2 + \alpha_p \|J^i X\|^2$, where α_V and α_p are regularization parameters to be determined (see below). For notational convenience, the regularization term is denoted globally as

$$\sum_i \|R_i X\|^2 \ .$$

In summary, we propose to solve the Laplace-Cauchy problem by minimizing

$$\|MX - m\|^2 + \sum \|R_i X\|^2 \tag{12}$$

under the constraint $HX = 0$. As explained above, we consider X to be an orthogonal projection of Y to the null space of H

$$X = P_{\mathcal{N}(H)} Y \ , \tag{13}$$

which allows us to cast the problem as an unconstrained minimization. Denoting $\tilde{M} = M P_{\mathcal{N}(H)}$ and $\tilde{R}_i = R_i P_{\mathcal{N}(H)}$, we minimize

$$\|\tilde{M} Y - m\|^2 + \sum \|\tilde{R}_i Y\|^2 \ . \tag{14}$$

A solution $\hat{Y}$ of (14) must satisfy

$$\left[\tilde{M}^T \tilde{M} + \sum \tilde{R}_i^T \tilde{R}_i\right] \hat{Y} = \tilde{M}^T m \ .$$

A unique least-squares solution of the above equation is obtained using the pseudoinverse, and a minimizer X of (12) then results from the projection $\hat{X} = P_{\mathcal{N}(H)} \hat{Y}$. From $\hat{X}$ the potential and the flux of each surface can be extracted using (11). The different steps of this Laplace-Cauchy method are outlined in Algorithm 2.

The choice of regularization parameters α_V and α_p is done using the L-curve method [14]. For a single-parameter minimization problem, the L-curve shows the log of the smoothing term versus the log of the residual term for all values of the regularization parameter. The curve displays a sharp corner (a maximum curvature point), corresponding to a recommended value of the regularization parameter. In our case, we iteratively apply the L-curve method to determine the two regularization parameters α_V and α_p by keeping one of them fixed and optimizing the other one in an alternating manner. Another option would be to use an L-surface [6], a generalization of the L-curve for multiple parameters.

Algorithm 2 Laplace-Cauchy

Inputs: meshes of surfaces $S_0, S_1, \dots S_N$, conductivities $\sigma_1, \dots, \sigma_N$
sensor positions x, measurements m
regularization parameters α_V, α_p

$P_{\mathcal{N}(H)} = \text{NullSpaceProjector}(S_0, S_1, \dots S_N, \sigma_1, \dots, \sigma_N)$;
$M = \text{SensorInterpolation}(S_0, x)$
$\tilde{M} = M\, P_{\mathcal{N}(H)}$
for $i = 0$ to N **do**
  $(G_i^1, G_i^2, G_i^3) = \text{P1SurfaceGradient}(S_i)$
  $(J_i^1, J_i^2, J_i^3) = \text{P0SurfaceGradient}(S_i)$
  for $j = 1$ to 3 **do**
    $\tilde{G}_i^j = G_i^j\, P_{\mathcal{N}(H)}$
    $\tilde{J}_i^j = J_i^j\, P_{\mathcal{N}(H)}$
  end for
end for
Find pseudoinverse solution $\hat{Y}$ of

$$\left[\tilde{M}^T\,\tilde{M} + \sum_{i=0}^{N}\sum_{j=1}^{3} \alpha_V (\tilde{G}_i^j)^T\,\tilde{G}_i^j + \alpha_p (\tilde{J}_i^j)^T\,\tilde{J}_i^j\right]\hat{Y} = \tilde{M}^T\, m$$

$\hat{X} = P_{\mathcal{N}(H)}\,\hat{Y}$
Return $V_0, V_1, \dots, V_N$ and $p_1, \dots, p_N$ extracted from $\hat{X}$

4. Numerical Experiments

We show the performance of our method on the cortical mapping problem. We have generated several sets of simulated datasets based on a simplified, spherical model, as well as on a realistic anatomy. The datasets are chosen so that comparison with previous published results is possible. We have calculated the electric potential and flux using a forward method [20] from known sources and added a Gaussian noise to the simulated scalp electrode measurements. Finally, we have estimated the cortex potential and flux from the scalp measurements using the Laplace-Cauchy method presented in Section 3 and we have evaluated the reconstruction error.

4.1. EEG model

Nested volumes of homogeneous conductivity are commonly used for EEG modelling. The number of nested volumes varies among models, from three (brain - skull - scalp) or four (brain - cerebrospinal fluid - skull - scalp), up to eleven for the most complex [15]. The possible anisotropy of the conductivities is not addressed here, nor is the estimation of the conductivity values. In our experiments, we used two

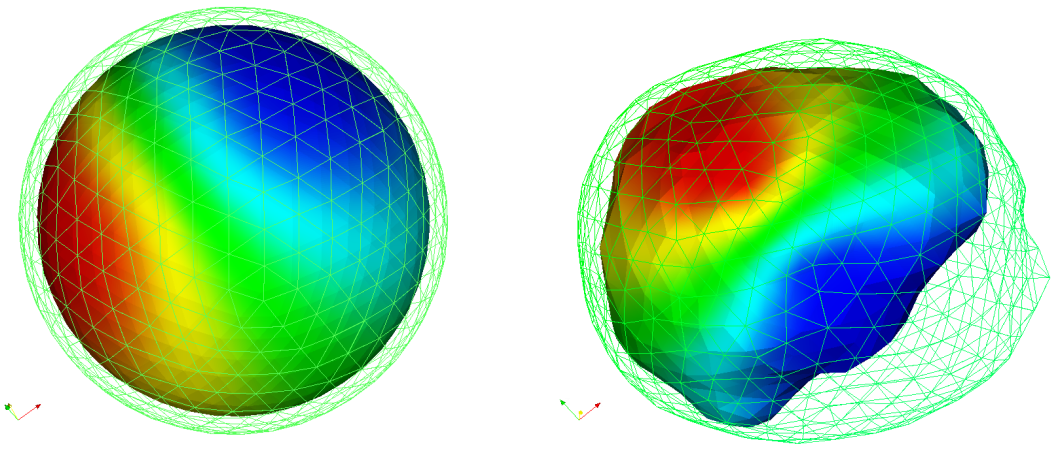

(a) spherical model (b) realistic model

Figure 2. The outer scalp surface (meshed) and the outer skull surface (on which a potential field has been mapped) for the two types of models considered in the simulations.

different three-layer models, whose outer two layers are represented in Figure 2:

(i) a spherical model, with three spheres of radii $(0.87, 0.92, 1)$ and conductivities $(1, 1/80, 1)$, representing the brain, the skull and the scalp surfaces, triangulated using 642 vertices (1280 triangles) per sphere; a set of 128 electrodes was positioned on the upper hemisphere;

(ii) a realistic head model obtained by segmenting a Magnetic Resonance Image (MRI) into three regions (brain, skull and scalp) to which standard conductivity values were assigned (1, 1/80, 1, respectively). The scalp, skull and brain surfaces were triangulated using 616, 510, and 510 vertices, respectively; two sets of electrodes, with 64 or 128 sensors, were positioned on the upper scalp surface.

For the spherical head model, we used three source configurations corresponding to the numerical experiments of He et al. [9]:

(i) a single tangential dipole with eccentricity of 0.65, at an angle $\pi/6$ with respect to z-axis;

(ii) two tangential dipoles with eccentricity of 0.65, each of which is at an angle $\pi/7$ with respect to z-axis;

(iii) one dipole at $(0.15, 0, 1.65)$ pointing to $+x$ direction and two dipoles located at $(0, \pm 0.4, 0.5)$ pointing in $+z$ direction.

For the realistic head model, a source configuration composed of two dipoles was designed to mimick Evoked Auditory Activity, i.e. two dipoles symmetrically placed in each hemisphere, close to the auditory cortices. The resulting scalp potential, displayed in Figure 4 (upper left), ressembles that of a single, centrally located dipole, as well as the potential on the skull (same figure, left picture on the second line). Only on the

surface of the cortex does the map appear bi-focal (Figure 4, third line), illustrating the inherent difficulty of the Cauchy problem.

4.2. Cortical mapping results

The results of the numerical experiments are presented in Tables 1 and 2 and in Figures 3 and 4. Since the experiments were synthetic, we had ground truth data to which reconstructions could be compared. In the sequel we refer to the ground truth simulated data as "true" data.

The relative error RE for the potential on a given surface is measured by:

$$\frac{\|V_{\text{rec}} - V_{\text{true}}\|_2}{\|V_{\text{true}}\|_2} = \frac{\left(\sum_{i\in\text{vertices}} \left(V_{\text{rec}}(i) - V_{\text{true}}(i)\right)^2\right)^{1/2}}{\left(\sum_{i\in\text{vertices}} \left(V_{\text{true}}(i)\right)^2\right)^{1/2}} , \tag{15}$$

and the relative error for the flux on a given surface is measured by:

$$\frac{\|p_{\text{rec}} - p_{\text{true}}\|_2}{\|p_{\text{true}}\|_2} = \frac{\left(\sum_{j\in\text{triangles}} \left(p_{\text{rec}}(j) - p_{\text{true}}(j)\right)^2\right)^{1/2}}{\left(\sum_{j\in\text{triangles}} \left(p_{\text{true}}(j)\right)^2\right)^{1/2}} . \tag{16}$$

To measure the topographical similarity between the reconstructed and true fields, we use the correlation coefficient (CC); for the potential, the CC is

$$\frac{\langle V_{\text{rec}},\, V_{\text{true}}\rangle}{\|V_{\text{rec}}\|_2\, \|V_{\text{true}}\|_2} = \frac{\sum_{i\in\text{vertices}} V_{\text{rec}}(i)\cdot V_{\text{true}}(i)}{\|V_{\text{rec}}\|_2\, \|V_{\text{true}}\|_2} , \tag{17}$$

and the CC for the flux is given by

$$\frac{\langle p_{\text{rec}},\, p_{\text{true}}\rangle}{\|p_{\text{rec}}\|_2\, \|p_{\text{true}}\|_2} = \frac{\sum_{j\in\text{triangles}} p_{\text{rec}}(j)\cdot p_{\text{true}}(j)}{\|p_{\text{rec}}\|_2\, \|p_{\text{true}}\|_2} , \tag{18}$$

The REs and CCs on the scalp, skull and cortex surfaces are reported in Tables 1 and 2. The values corresponding to the flux on the scalp are not reported since our model assumes the flux to vanish (see Section 2.1). Notice that the addition of noise (as a percentage of the standard deviation of the scalp measurements), does not degrade the results for the spherical head model as much as for the realistic head model. The potential reconstruction is more accurate on the scalp and skull surfaces than on the cortex: inaccuracies are amplified with the crossing of layers.

To appreciate the quality of the results, one must bear in mind the very few data terms available (64 or 128) compared to the number of reconstructed terms (4486 for the spherical model, and 3668 for the realistic model).

Figures 3 and 4 present the true and reconstructed solutions, for the spherical head model and source model 2 (Figure 3) and for the realistic head model with auditory source model (Figure 4). This makes it possible to appreciate the topography of the fields and of their reconstructions: visually, the reconstructed fields and the true fields are spatially quite close. This is in particular evident in the realistic case, Figure 4, where two focussed patches of electrical activity have correctly been estimated on the cortex, although on the scalp only one local maximum was present. One can also note the quality of the scalp potential reconstruction, even in the presence of noise.

Head model	Source	Noise	V_{scalp}	V_{skull}	V_{cortex}	p_{skull}	p_{cortex}
spherical (128 electrodes)	**1**	**0%**	**0.0493**	**0.0935**	**0.4250**	**0.3909**	**0.4767**
		10%	0.0712	0.0973	0.5020	0.4261	0.4937
		20%	0.1319	0.1880	0.6957	0.5701	0.5838
spherical (128 electrodes)	**2**	**0%**	**0.0291**	**0.0332**	**0.4521**	**0.3184**	**0.4069**
		10%	0.0655	0.0770	0.5392	0.3950	0.4497
		20%	0.1194	0.1526	0.7562	0.5841	0.5723
spherical (128 electrodes)	**3**	**0%**	**0.0479**	**0.0896**	**0.4878**	**0.4922**	**0.5672**
		10%	0.0685	0.1022	0.5594	0.5269	0.5841
		20%	0.1228	0.1642	0.7444	0.6550	0.6638
realistic (64 electrodes)	**auditory**	**0%**	**0.0416**	**0.1406**	**0.5026**	**0.4188**	**0.5226**
		5%	0.0664	0.1630	0.6149	0.5222	0.5890
realistic (128 electrodes)	**auditory**	**0%**	**0.0238**	**0.0580**	**0.4858**	**0.3466**	**0.4788**
		5%	0.0404	0.0694	0.6009	0.4333	0.5245

Table 1. Relative errors, on each surface, measured by (15) and (16), for each head and source model described in the text.

Head model	Source	Noise	V_{scalp}	V_{skull}	V_{cortex}	p_{skull}	p_{cortex}
spherical (128 electrodes)	**1**	**0%**	**0.9988**	**0.9956**	**0.9055**	**0.9240**	**0.8846**
		10%	0.9975	0.9943	0.8705	0.9049	0.8725
		20%	0.9915	0.9800	0.7886	0.8329	0.8153
spherical (128 electrodes)	**2**	**0%**	**0.9996**	**0.9995**	**0.8927**	**0.9511**	**0.9170**
		10%	0.9979	0.9970	0.8443	0.9182	0.8936
		20%	0.9929	0.9882	0.7266	0.8287	0.8263
spherical (128 electrodes)	**3**	**0%**	**0.9989**	**0.9960**	**0.8882**	**0.8739**	**0.8260**
		10%	0.9978	0.9947	0.8309	0.8501	0.8121
		20%	0.9926	0.9866	0.7043	0.7684	0.7530
realistic (64 electrodes)	**auditory**	**0%**	**0.9993**	**0.9901**	**0.8650**	**0.9081**	**0.8530**
		5%	0.9980	0.9849	0.7958	0.8594	0.8109
realistic (128 electrodes)	**auditory**	**0%**	**0.9997**	**0.9983**	**0.8750**	**0.9390**	**0.8807**
		5%	0.9992	0.9972	0.8047	0.9014	0.8515

Table 2. Correlation coefficients, on each surface, measured by (17) and (18), for each head and source model described in the text.

5. Discussion

We have proposed a new Tikhonov-based boundary element solution for the Cauchy transmission problem. The boundary element method is based on a mixed formulation, involving both the potential and the flux. We have applied it in the field of encephalography, where it offers a "cortical mapping" solution involving both the potential and the normal current, which no previous method had achieved in this field. It promises to be very useful as a preprocessing step before applying inverse source

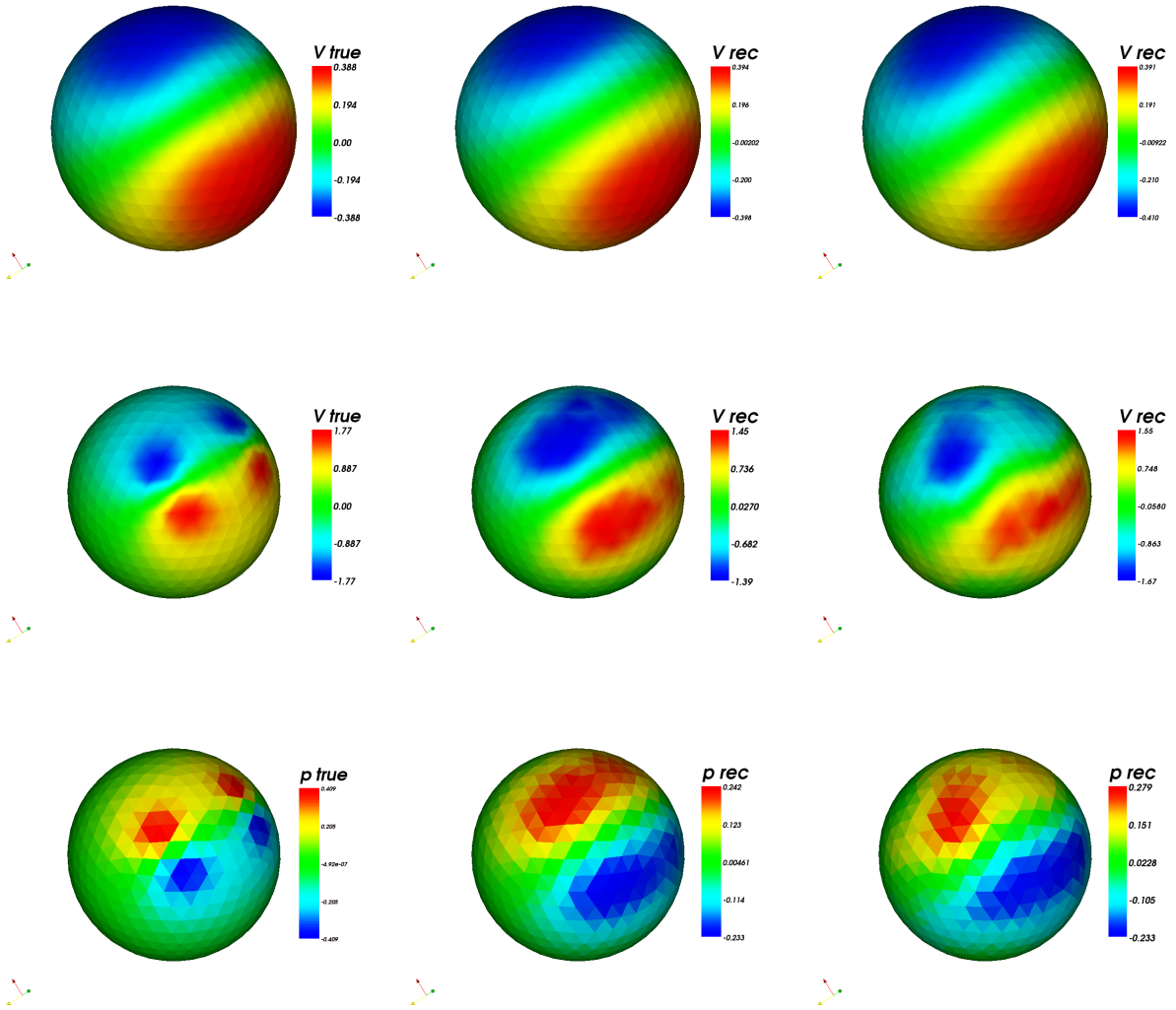

(a) true solution (b) solution with 0% noise (c) solution with 20 % noise

Figure 3. Spherical head model and source model 2: 3D rendering of the potential on the scalp (top line), the potential on the cortex (middle line) and the flux on the cortex (bottom line). Each of the surfaces is discretized with 642 vertices and 1280 triangles, and 128 electrodes are placed on the scalp

localization procedures such as described in [4] or in [5], which require transmission of Cauchy data up to the cortical surface. According to simulations [13], the precision of the cortical mapping is sufficient for source localization via rational approximation.

Acknowledgments

The authors were partially funded by a PAI Barrande grant from the French Ministry of Foreign affairs and Czech Ministry of Education. The second author was sponsored by the Czech Ministry of Education under Project MSM6840770012. We acknowledge enlightening discussions with Jean-Michel Badier, Juliette Leblond and Jean-Paul

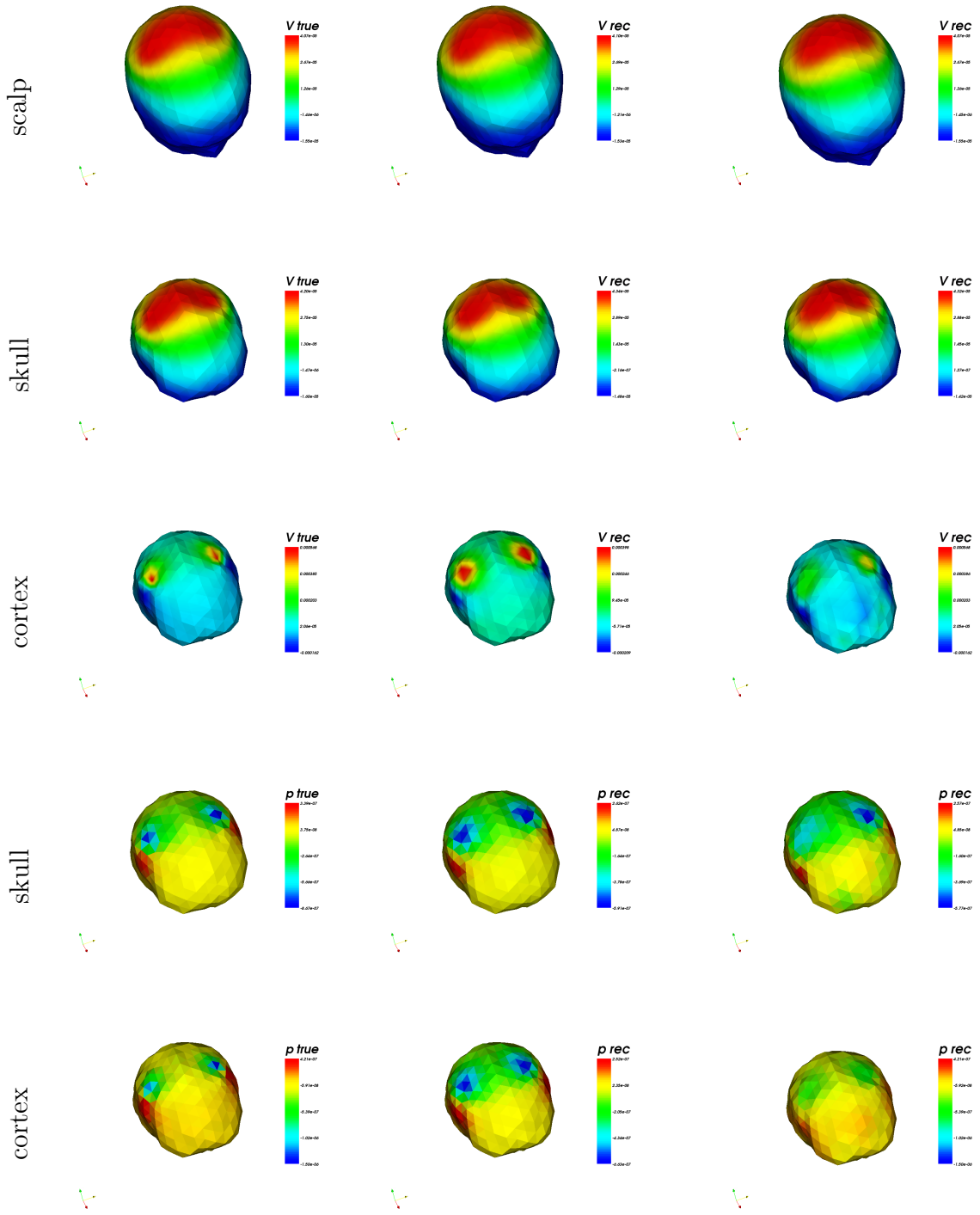

(a) true solution (b) solution with 0% noise (c) solution with 5 % noise

Figure 4. Realistic head model and auditory source model: 3D rendering of the potential and the flux on the scalp and on the cortex. The head is viewed from above, with the nose pointing downwards.

Marmorat, and we are very grateful to the reviewers for their constructive comments.

References

[1] G. Adde, M. Clerc, and R. Keriven. Imaging methods for MEG/EEG inverse problem. In Jaakko Malmivuo, editor, *International Journal of Bioelectromagnetism*, volume 7, pages 111–114, 2005.

[2] S. Andrieux, T.N. Baranger, and A. Ben Abda. Solving Cauchy problems by minimizing an energy-like functional. *Inverse Problems*, 22:115–133, 2006.

[3] M. Azaiez, F. Ben Belgacem, and H. El Fekih. On Cauchy's problem: II. completion, regularization and approximation. *Inverse Problems*, 22:1307–1336, 2005.

[4] A. El Badia and T. Ha-Duong. An inverse source problem in potential analysis. *Inverse Problems*, 16:651–663, 2000.

[5] L. Baratchart, A. Ben Abda, F. Ben Hassen, and J. Leblond. Recovery of pointwise sources or small inclusions in 2D domains and rational approximation. *Inverse Problems*, 21:51–74, 2005.

[6] M. Belge, M. Kilmer, and E. Miller. Efficient determination of multiple regularization parameters in a generalized L-curve framework. *Inverse Problems*, 18:1161–1183, 2002.

[7] F. Ben Belgacem and H. El Fekih. On Cauchy's problem: I. a variational Steklov-Poincar'e theory. *Inverse Problems*, 21:1915–1936, 2005.

[8] F. Berntsson and L. Eldén. Numerical solution of a Cauchy problem for the Laplace equation. *Inverse Problems*, 17:839–853, 2001.

[9] B.He, X. Zhang, J. Liang, H. Sasaki, D. Wu, and V.L. Towle. Boundary Element Method-based cortical potential imaging of somatosensory evoked potentials using subjects' Magnetic Resonance Images. *NeuroImage*, 16:564–576, 2002.

[10] Marc Bonnet. *Boundary Integral Equations Methods for Solids and Fluids.* John Wiley and Sons, 1999.

[11] L. Bourgeois. A mixed formulation of quasi-reversibility to solve the Cauchy problem for Laplace's equation. *Inverse Problems*, 21:1087–1104, 2005.

[12] A. Cimetière, F. Delvare, M. Jaoua, and F. Pons. Solution of the Cauchy problem using iterated Tikhonov regularization. *Inverse Problems*, 17:553–570, 2001.

[13] M. Clerc, B. Atfeh, J. Leblond, L. Baratchart, J.-P. Marmorat, T. Papadopoulo, and J. Partington. The Cauchy problem applied to cortical imaging: comparison of a boundary element and a bounded extremal problem. In Christoph Michel D. Brandeis, T. Koenig, editor, *Brain Topography*, volume 18. Springer Science and Business Media B.V., October 2005.

[14] Per Christian Hansen. *Rank-deficient and discrete ill-posed problems: Numerical aspects of linear inversion.* SIAM Monographs on Mathematical Modeling and Computation. SIAM, Philadelphia, 1998.

[15] J. Haueisen, D.S. Tuch, C. Ramon, P.H. Schimpf, V.J. Wedeen, J.S. George, and J.W. Belliveau. The influence of brain tissue anisotropy on human EEG and MEG. *NeuroImage*, 15:159–166, 2002.

[16] Bin He, Yunhua Wang, and Dongsheng Wu. Estimating cortical potentials from scalp EEGs in a realistically shaped inhomogeneous head model by means of the boundary element method. *IEEE Transactions on Biomedical Engineering*, 46(10):1264–1268, October 1999.

[17] Gabriele Inglese. An inverse problem in corrosion detection. *Inverse Problems*, 13:977–994, 1997.

[18] Michael V. Klibanov and Fadil Santosa. A computational quasi-reversibility method for Cauchy problems for Laplace's equation. *SIAM J. Appl. Math.*, 51(6):1653–1675, December 1991.

[19] V.A. Kozlov, V.G. Mazya, and A.V. Fomin. An iterative method for solving the Cauchy problem

for elliptic equations. *Comput. Maths. Marh. Phys.*, 31(1):45–52, 1992.

[20] J. Kybic, M. Clerc, T. Abboud, O. Faugeras, R. Keriven, and T. Papadopoulo. A common formalism for the integral formulations of the forward EEG problem. *IEEE Transactions on Medical Imaging*, 24:12–28, jan 2005.

[21] J. Kybic, M. Clerc, O. Faugeras, R. Keriven, and T. Papadopoulo. Generalized head models for MEG/EEG: boundary element method beyond nested volumes. *Phys. Med. Biol.*, 51:1333–1346, 2006.

[22] Jean-Claude Nédélec. *Acoustic and Electromagnetic Equations*. Springer Verlag, 2001.

[23] C. Tandonnet, B. Burle, T. Hasbroucq, and F. Vidal. Spatial enhancement of EEG traces by surface Laplacian estimation: comparison between local and global methods. *Clinical Neurophysiology*, 116(1):18–24, 2005.